# 1 Introduction

Many applications in machine vision and photogrammetry involve taking measurements from images. Examples of image metrology applications include, in medicine: image-guided surgery and multimode imaging; in robotics: calibration, object tracking, and mobile robot navigation; in industrial automation: component alignment, for example for electronic assembly, and reading 2-D bar codes; and in dynamic testing: measurements from high-speed images. In these applications, landmarks are detected and computer algorithms are used to determine their location in the image. When landmarks are located there is, of course, a degree of uncertainty in the measurement. This uncertainty is the subject of this work.

Examples of landmarks used for metrology are shown in Figures 1.1–1.4. In Figure 1.1, we see a standard artificial landmark on the head of the crash test dummy. Quadrature landmarks such as this one are recorded in high-speed images during tests, and by locating the landmarks, measurements of motions can be taken from the images. In another application, landmarks such as those seen in Figure 1.2 are sometimes implanted for medical imaging prior to surgery. Fiducial marks are landmarks used for registration. This and other terms are defined in a glossary provided in Appendix B. Amongst other uses, these fiducial marks in medical images and associated image-based measurement tools can permit the surgeon to

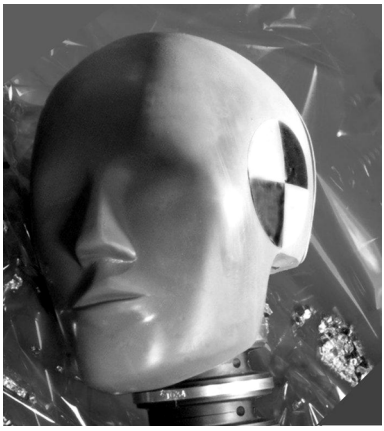

**Figure 1.1.** Crash test dummies carry *artificial* landmarks to improve the accuracy of motion measurements from images (Photo courtesy of NASA)

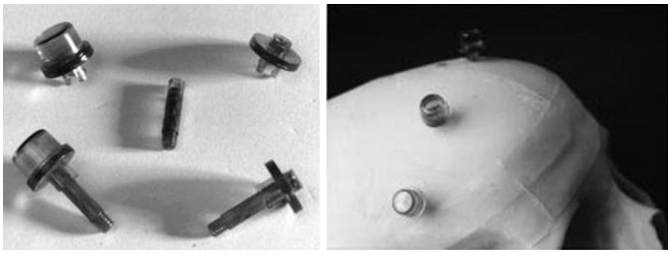

**Figure 1.2.** Fiducial markers for implanting and precision location in medical images. These markers produce circular patterns in CAT images (Images courtesy of IEEE, from C.R. Mauer *et al.*, "Registration of head volume images using implantable fiducial markers," IEEE Trans. Medical Imaging, Vol. 16, No. 4, pp. 447–462, 1994).

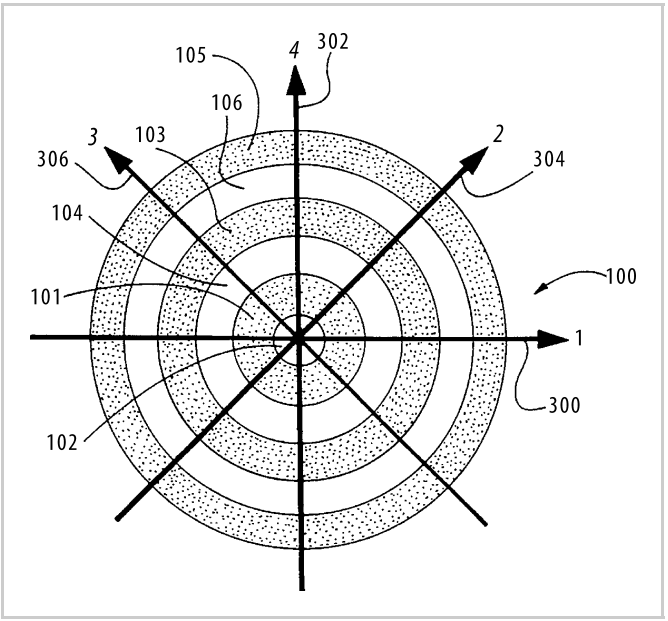


**Figure 1.3.** Bullseye landmark for robust detection and precision location. This is the landmark used for reading bar-codes on UPS labels. This is the landmark used for reading bar-codes on UPS labels (From U.S. patent 5,515,447, "Method and apparatus for locating an acquisition target in two-dimensional images …").

coordinate the patient on the operating table with 3-D medical images, guiding the way to structures that cannot be seen from the surface. When these tools are used in the operating room, the precision of landmark location plays a role in determining the working volume of the camera-based measurement system, and the flexibility to locate the system out of the surgeon's way. Other examples of landmarks used for industrial metrology or as part of a bar-code reader can be seen in Figures 1.3 and 1.4.

Photogrammetry is the science of spatial measurement from images. In photogrammetry, artificial landmarks can be used to mark and locate features for measurement. Machine vision finds application in many industries where landmarks are used for alignment and inspection. Plate 1 (see Color Section, page 145)

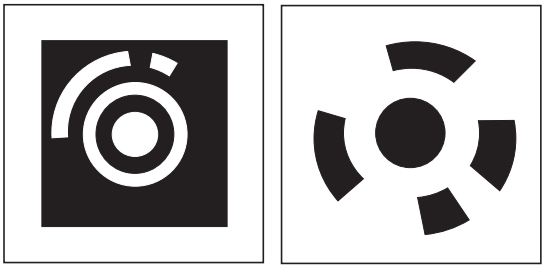

**Figure 1.4.** Artificial landmarks for metrology (Images courtesy of G. Ganci, H. Handley, "Automation in videogrammetry," Melbourne, FL: Geodetic Services Inc.)

shows artificial landmarks used for alignment or measurement steps in the printing and electronic industries.

The digital images considered in this work are broken into pixels, or picture elements, which are the individual samples of the scene, as seen in Figure 1.5. The challenge of landmark location is to accurately estimate the projection in the image of the center of the landmark. Figure 1.5 illustrates the case where the landmark occupies relatively few pixels, which is the most challenging case and a common one in image measurement applications, because space is limited in both the image and in the scene in which the landmark lies. The measured intensity levels, one quantized value per pixel, are the data available for landmark location estimation.

Automated assembly and inspection, vision-guided robotic manipulation, photogrammetry, image metrology and camera calibration all benefit from precise landmark location, and so it is useful to know how accurately artificial landmarks can be located digital images. It is well known that subpixel accuracy can be achieved; but to answer the question of whether a landmark can be located with an accuracy of $\pm 0.1$, 0.01 or 0.001 pixels requires detailed consideration. This work aims to answer the question of landmark location precision by establishing the theoretical minimum uncertainty that any location estimator can achieve, by developing tools for evaluating the uncertainty of practical estimators, and by presenting an experiment for directly measuring landmark location precision. The fruits of these labors can be used to determine the accuracy of a specified system, or to engineer a system to meet an accuracy goal. As O'Gorman *et al.* point out,

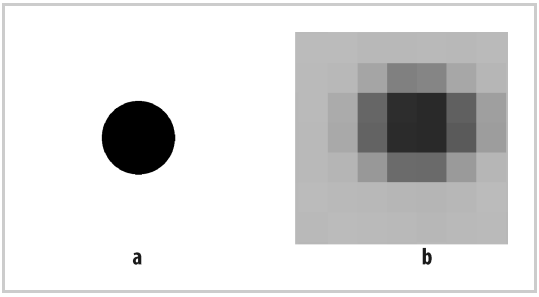


**Figure 1.5a,b.** Circular landmark; **a** ideal image of the landmark, **b** digital image of the landmark. Each picture element of the digital image corresponds to a measured intensity level (or three measured intensities for color images).

"… the benefits of methods that achieve subpixel precision can be seen from two perspectives: either as a means to obtain a higher precision, or as a means to obtain the same precision at less computational cost." (O'Gorman *et al.* 1990).

Since the present work is quite narrowly focused, it is worth mentioning what the present work is not. It is not a study of the entire range of questions that arise when measuring from images. In particular, the question of how a landmark is detected is neglected. For automated image processing this is an important and challenging question, but for the present purposes it is assumed that the presence of the landmark in the image is known, along with its approximate location. Furthermore, the sources of uncertainty considered are restricted to those that arise with the imaging and estimation processes, which is to say that any uncertainty in the shape of the landmark itself is neglected. This is effectively a restriction to well-made artificial landmarks. Indeed, in the numerical and experimental studies of the present report only planar-circular landmarks are considered, although the methods extend to other shapes. Here, the only concern is with the location of the landmark in the image, and so, although the numerical tool incorporates a lens distortion model, displacement of the landmark in the image due to lens distortion does not affect the conclusions. Finally, only digital images are considered; that is, images that are quantized both in space (pixels) and intensity. This is more a challenge than a simplification, since the main theoretical challenge of this work is to deal with quantization processes when determining the uncertainty. Narrowly focused as it is, the present work does have these chief aims:

1. To introduce a measure for landmark location uncertainty that overcomes the nonstationary statistics of the problem.
2. To develop an extended model for the physics of image formation, capturing aspects of the physical process that contribute to the determination of the uncertainty.
3. To establish the Cramér–Rao lower bound (CRLB) for the uncertainty of landmark location, given a description of the landmark and imaging configuration. The CRLB establishes a minimum level of uncertainty for any unbiased estimator, independent of the algorithm used.
4. To build a set of tools for analyzing the uncertainty of practical landmark and imaging configurations and location estimation algorithms, taking into account the spatial and intensity quantization in the image and the nonstationary nature of the statistics in particular.
5. To demonstrate new, model-based landmark location estimators that perform near the Cramér–Rao theoretical limit.
6. To validate these tools by developing and executing an experiment that can directly measure the uncertainty in landmark location estimates. The principal challenge to experimental validation is to provide a means to separately and accurately establish the true location of a landmark in the image.

These six goals form the basis for the remainder of the work.

## 1.1 Prior Art

Landmark location uncertainty has been studied for many years by numerous investigators of photogrammetry and machine vision. The methods used by scientists to approach landmark location uncertainty problems can be divided into two major categories: statistical and geometrical.

The first approaches used statistical approximation for the quantization and sampling errors and then applied well-established statistical techniques (Förstner 1982; Dvornychenko 1983). Gonsalves (1976), Ho (1983), Ryan *et al.* (1982), and Sriraman *et al.* (1989) modeled the entire digital image as a stochastic process so that statistical analysis could be used to determine the bounds for the error variances.

As a variation on the statistical approaches, several authors explored the use of autocorrelation peak searching with known landmark templates. Tian and Hunhns (1986) studied correlation interpolation and non-noisy intensity interpolation on synthetic images; that is, images created artificially following a deterministic mathematical model. They concluded that the major factors affecting landmark location uncertainty are the choice of interpolation function (based on the model used), the spatial sampling density (resolution), and the amplitude quantization level (gray level). The drawback of this methodology is that it requires a descriptive model of the image to be analyzed, not just the landmark. Nishihara and Crossley (1988) developed and implemented a similar technique that was applied to the alignment of photolithographic images in integrated circuit manufacturing. The authors analyzed the effects of noisy images on the location uncertainty. In this case, the application features a controlled environment where the model of the image (size, shape, and orientation) is known in advance.

Similarly, Cox *et al.* (1990) addressed the problem of subpixel landmark location for surface-mounted printed circuit board (PCB) assembly operation by developing an algorithm that used the model of an image as a reference for a 2-D matching search to predict the error in the measurement. A variation on the above methods was introduced by Tichem and Cohen (1994), where the centroid and model of a circularly symmetric landmark was used as a seed for the matching algorithm. This study recognized the difficulty of landmark location when the landmark is not coplanar with the imager, so that the landmark image is altered by perspective distortion.

Parametric modeling of the landmark was used initially by Duda and Hart (1972), Shapiro (1978), Yam and Davis (1981), and Ballard (1981), with emphasis placed on landmark detection via the use of Hough transforms and little attention paid to the landmark location uncertainty problem. Several other authors, such as Thurgood and Mikhail (1982) and Hachicha *et al.* (1989), used parametric modeling of particular landmark models to infer landmark location uncertainty from statistical properties of the parameter estimates. This technique was applied successfully by Tabatabai and Mitchell (1984) and Nalwa and Binford (1986) in the precision edge location application.

In contrast to statistical methodologies, analytic techniques used in landmark location have focused on geometric approaches. The first generation of these

**Table 1.1.** Mapping of relevant publications vs. key elements for landmark location uncertainty

| | | Landmark Geometry | Intensity Quantization | Imager Noise | Smoothing Effects |
|---|---|---|---|---|---|
| **Statistical Modeling** | Widrow (1965) | | × | | |
| | Duda and Hart (1972) | | | | |
| | Gonsalves (1976) | | × | | |
| | Shapiro (1976) | | | | |
| | Ballard (1981) | | | | |
| | Ryan *et al.* (1982) | | | | |
| | Förstner (1982) | | | | |
| | Thurgood and Mikhail (1982) | × | | | |
| | Dvornychenko (1983) | | | | |
| | Ho (1983) | | | | |
| | Doros (1984) | × | | | |
| | Nielsen *et al.* (1984) | | × | | |
| | Tabatabai and Mitchell (1984) | × | | | |
| | Nalwa and Binford (1986) | × | | | × |
| | Bruckstein (1987) | | × | | |
| | Nishihara and Crossley (1988) | | | | |
| | Hachicha *et al.* (1988) | | | | |
| | Sriraman *et al.* (1989) | | | | |
| | Tian and Huhns (1990) | | | | |
| | Cox *et al.* (1990) | | | | |
| | Tichem and Cohen (1994) | × | | | |

**Table 1.1.** (continued)

| | | Landmark Geometry | Intensity Quantization | Imager Noise | Smoothing Effects |
|---|---|---|---|---|---|
| **Geometric Approaches** | Klassman (1975) | × | | | |
| | Kulpa (1979) | × | | | |
| | Hyde and Davis (1983) | × | × | | |
| | Nakamura and Aizawa (1984) | × | | | |
| | Dorst and Smeulders (1986) | × | | | |
| | Berenstein *et al.* (1987) | × | | | |
| | Havelock (1989) | × | × | | |
| | Amir (1990) | × | | | |
| | O'Gorman *et al.* (1990) | × | | | |
| | Havelock (1991) | × | × | × | |
| | Bose and Amir (1990) | × | | | |
| | Kiryati and Bruckstein (1991) | × | × | | |
| | Chiorboli and Vecchi (1993) | × | × | | |
| | Efrat and Gotsman (1994) | × | | | |
| | O'Gorman (1996) | × | | | |
| | Bruckstein *et al.* (1998) | × | | | |
| | Bruckstein and Holt (1999) | × | | | × |

**Table 1.2.** Summary of research evolution for landmark location uncertainty

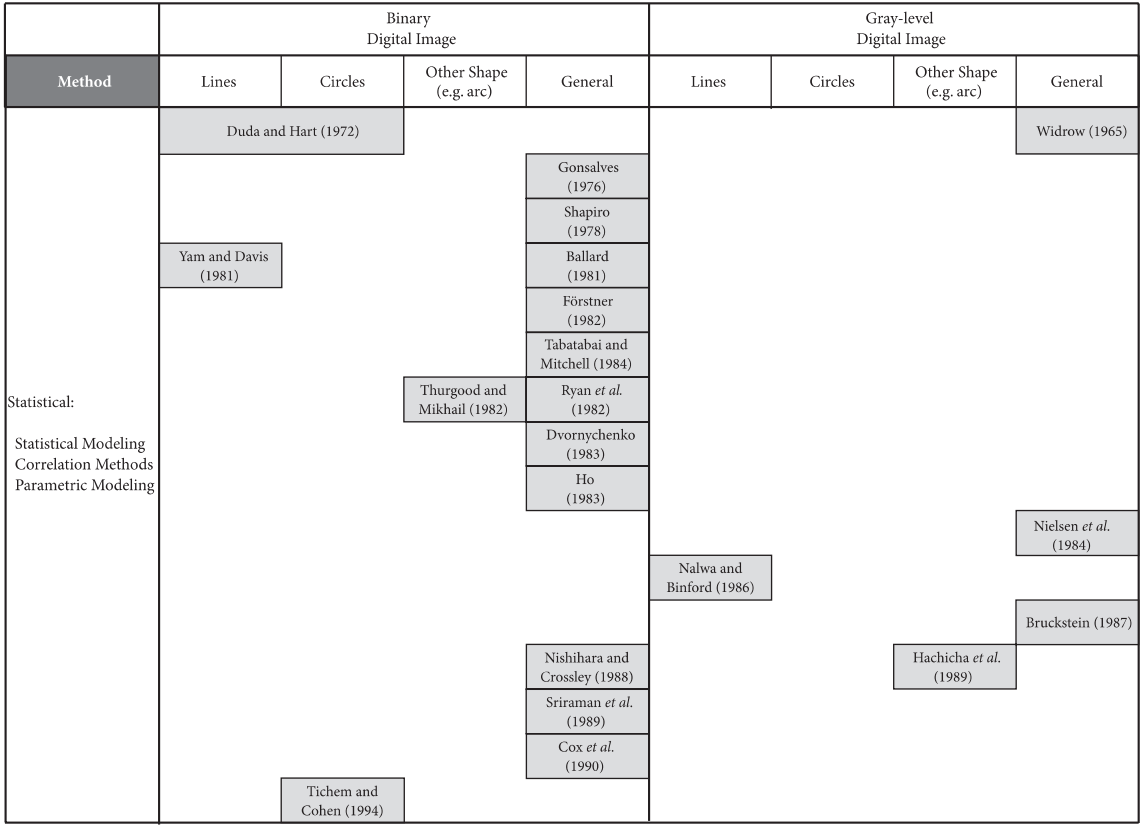

**Table 1.2.** (continued)

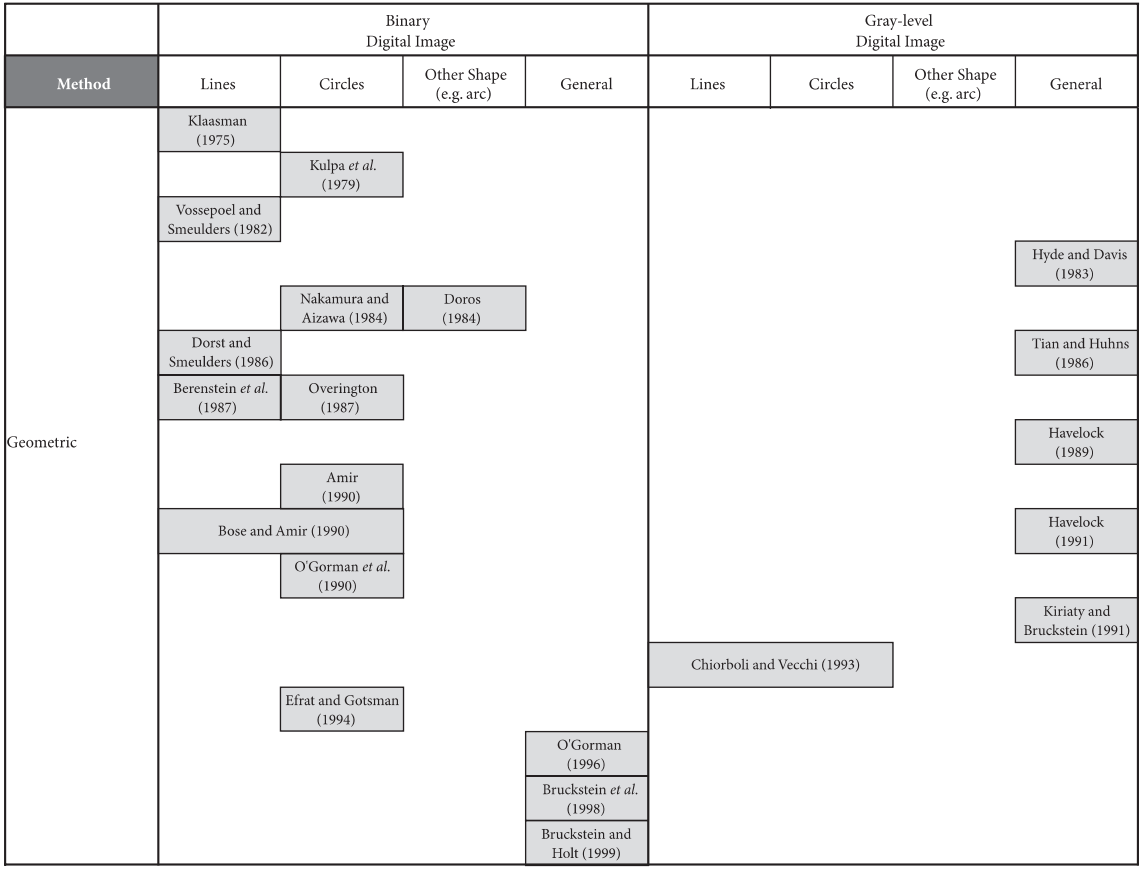

techniques was based on binary digital images, disregarding gray levels. Kulpa (1979) provided an in-depth geometrical analysis of the properties of digital circles, but Hill (1980) was the first to provide a rigorous geometrical analysis of landmark location uncertainty for a variety of geometrical shapes based on synthetic binary images. Subsequently, several investigators reported a variety of algorithms for improving error performance for particular landmark shapes. Vossepoel and Smeulders (1982), Dorst and Smeulders (1986), and Berenstein *et al.* (1987) focused on calculating uncertainty in the location of straight spatially quantized lines. Nakamura and Aizawa (1984) investigated the expansion of this work to circular landmarks, while Amir (1990) and Efrat and Gotsman (1994) presented new methodologies for locating the center of a circular landmark and Doros (1986) worked on the geometrical properties of the image of digital arcs. Bose and Amir (1990) investigated how landmark location uncertainty is affected by the shapes and sizes of the binary images of various landmarks, concluding that circular shapes provide superior performance. Similarly, O'Gorman (1990), O'Gorman *et al.* (1996), and Bruckstein *et al.* (1998) investigated novel shapes (bullseye and others), which improved the uncertainty performance for binary images.

The second generation of analytic techniques focused on the exploitation of the gray-level information, taking advantage of more bits in the intensity quantization. The use of grayscale intensity quantization improves landmark location uncertainty (Rohr 2001). One of the first algorithms to make use of grayscale information was developed by Hyde and Davis (1983), which gave results similar to the ones obtained for binary images. Klassman (1975) proved that for any finite spatial sampling density (density of pixels per area), the position uncertainty of a line was greater than zero, even when using unquantized images; that is, images whose amplitude is a continuous function. Kiryati and Bruckstein (1991) showed how location uncertainty performance on binary image could be improved by the use of gray-level digitizers. Chiorboli and Vecchi (1993) showed empirically that the uncertainty performance of the results from Bose and Amir could be improved by an order of magnitude by using gray-level information.

Of particular importance is the locale framework proposed by Havelock (1989, 1991) and expanded by Zhou *et al.* (1998). This methodology is based on the concept of regions of indistinguishable object position, called locales, caused by spatial and intensity quantization. In the absence of noise, an observed digital (quantized) image of a landmark corresponds to a region in which the true landmark may lie. In general, this is a many-to-one mapping; that is, many different landmark locations generate the same digital image. Havelock's work marked a great leap forward in analytic determination of landmark location uncertainty.

Table 1.1 shows how selected research publications address aspects of image formation that are important for landmark location uncertainty. A summary of the research evolution for landmark location uncertainty is shown in Table 1.2. As the table reflects, research has been directed toward understanding and reducing landmark location uncertainty for over three decades.

## 1.2 Modeling Image Formation

In this section, the approach of this work to modeling image formation is described. The goal is to capture the physical processes of image formation (such as properties of the camera and imager) that are important when determining the ultimate limits to landmark location uncertainty.

While many previous studies have focused on binary images, several investigators have recognized the need to develop methods for subpixel landmark location that make more efficient use of the information present in the image. Havelock (1989), a pioneer in the investigation of landmark location uncertainty, points out that "it is not trivial to answer these questions [of landmark location uncertainty with grayscale information] in a complete and meaningful way. This is a new area of investigation, with only few results available at present." Similarly, the work of Bruckstein *et al.* (1998) recommends further research into the exploitation of the gray-level information to improve precision in landmark location.

Grayscale information is only one of the characteristics that influence landmark location uncertainty. An extensive model of image formation comprises contributions from several scientific fields: physics (optics), electronics (imager), and computer science (image processing and estimation algorithms). The research framework presented here introduces a methodology to determine the minimal uncertainty bound in landmark location based on the Cramér–Rao lower bound. The CRLB methodology considers an extensive model of image formation, including six degree-of-freedom (DOF) landmark to camera geometry, diffraction, defocus, lens distortion, grayscale, pixel geometry, and pixel sensitive area. A list is shown in Figure 1.6 of the aspects of the image formation process that are considered in this work. The Cramér–Rao lower bound methodology provides a theoretical statistical minimum limit on the landmark location uncertainty. Knowledge of this bound provides the means to evaluate the actual performance of both existing and future landmark location estimators. With this model, a general framework is established to measure the uncertainty performance of existing landmark location estimators, *e.g.*, binary, geometrical, autocorrelation, statistical modeling, and others.

An important challenge to addressing uncertainty in landmark location is that the statistics of landmark location are not stationary. That is to say, the theoretical CRLB as well as the covariance and bias of practical estimators all depend on *where* the landmark falls on the imager. This characteristic is associated with the locales and raises the question of how to express uncertainty, since the covariance matrix itself varies significantly with small shifts of the true landmark location. A method is needed which averages over the range landmark locations and yet conveys information of practical engineering significance. At the same time, the method chosen to express uncertainty should be applicable to all three of the measures sought: the Cramér–Rao lower bound, analysis of practical estimators, and experimental measurement.

The confidence interval has been chosen to express landmark location uncertainty. The confidence interval is expressed as the radius of a circle in the digital image that will hold 95% (or in some cases 99%) of estimated landmark locations.

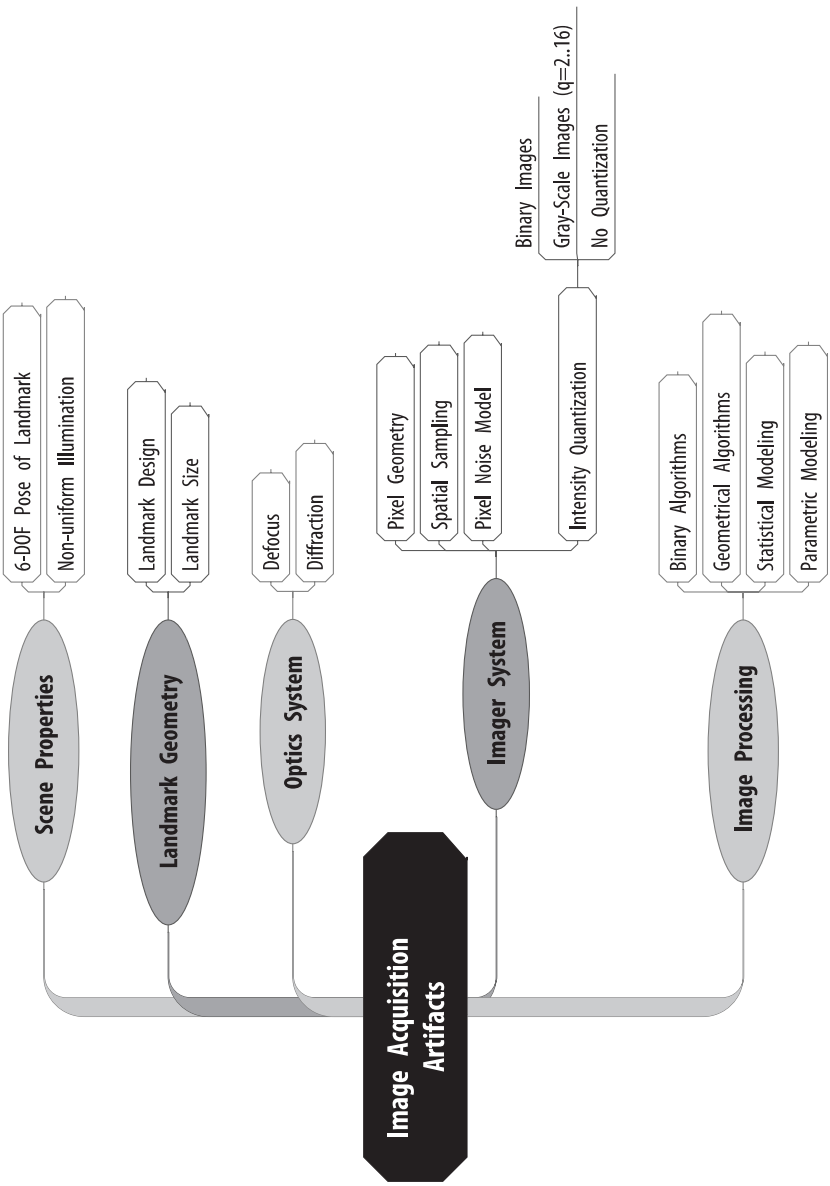


**Figure 1.6.** Contributors to the uncertainty bound in landmark location

In Chapter 3, methods for evaluating the confidence interval for the CRLB and analytic cases are described in detail. For the experimental data, the confidence intervals are obtained simply by determining the smallest circle that will enclose 95% of the data. While coordinates of millimeters or microns on the imager are preferred over pixel coordinates for image metrology, we have chosen to express the confidence interval in millipixels because landmark location estimators operate on pixel data. It is recognized that a circle measured in pixels translates, in general, to an ellipse in image coordinates.

Using the confidence intervals, results are summarized by means of performance maps. These maps are a graphical representation of the location uncertainty computed using the CRLB, or the analysis of a practical algorithm, or as measured by experiment. Each performance map corresponds to a particular set of model parameters, called a configuration. Figure 1.7 shows two examples of hypothetical landmark location estimation performance maps corresponding to two different configurations.

The landmark location estimation performance maps permit identification of the gap between existing algorithms and the minimal uncertainty bound. Furthermore, they pave the way for the creation of novel estimators that approach the bound by identifying the main image formation factors that contribute to the uncertainty bound.

The complexity of an extensive physical model of image formation, involving the characteristics shown in Figure 1.6, has been a barrier to the study of landmark location uncertainty. As we will see in the next chapter, to correctly determine the interaction of small displacements of the landmark and the corresponding small changes in the measured data, it is necessary to consider the finite sensitive

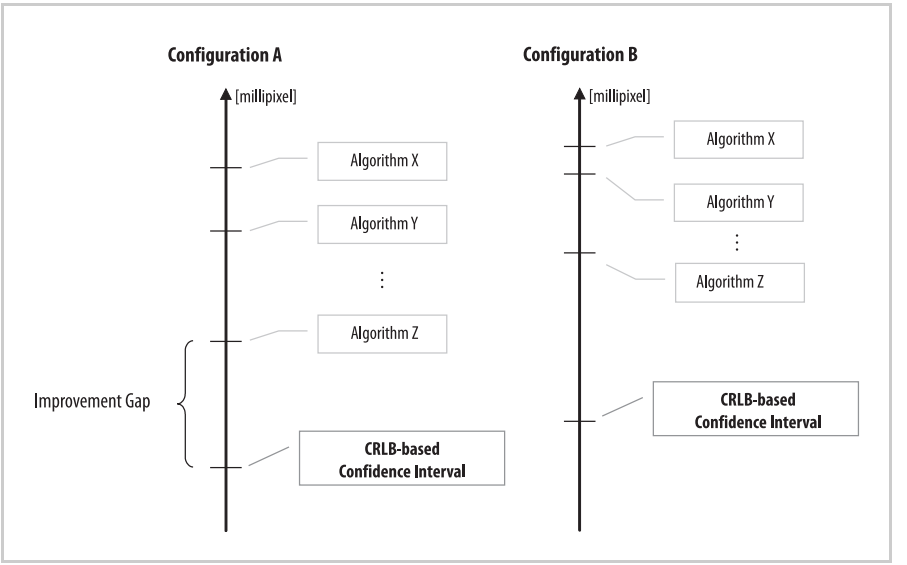


**Figure 1.7.** Hypothetical landmark location estimation performance maps

area of each pixel and also the smoothing of the image introduced by diffraction. Since the sensitivity of the image data to the landmark location is essential to this study, neither characteristic can be neglected. However, modeling finite sensitive area requires integration of the incident light intensity (called the illuminance function) over the two-dimensional sensitive area of each pixel, and this integral cannot be performed in closed form. Indeed, because of the 2-D convolution required to model diffraction-induced smoothing of the illuminance function, the illuminance function itself cannot be expressed in closed form for any case other than a straight edge.

The strategy used here to address these challenges employs a mix of analysis, where feasible, and numerical work where required. The inclusion of diffraction in the analysis of landmark location uncertainty is an important innovation, because the smoothing of the illuminance function by diffraction *enables* rigorous numerical analysis. In particular, the partial derivatives of the probability distributions of the measured data with respect to the location of the landmark, which are needed to compute the CRLB and also the performance of practical estimators, are well defined, well behaved, and can be computed only because diffraction assures us that the illuminance function has no discontinuities. This motivates the incorporation of diffraction as part of the model of image formation.

This work also introduces two novel circular landmark location estimation algorithms, which perform with confidence intervals at the tens of millipixels level. This level of uncertainty is several times lower than that of a more conventional centroid algorithm. These algorithms are demonstrated for circular landmarks, but the model-based methodology can be extended to accommodate other landmark designs.

The first new landmark location estimator is named the "ellipsoidal contour" algorithm. It exploits the gray-level information present in the image by identifying points on a grayscale contour around the landmark, and then estimating the parameters of an ellipse fit to the contour. The second estimator, named "Butterworth tepuy", also exploits gray-level information by creating a parametric model of the intensity surface of the landmark, while considering the smoothing caused by diffraction.

To experimentally measure the uncertainty of a landmark location algorithm, it is necessary to have an independent measurement of the true location in the image of the landmark. This challenge is met by designing a second artwork that surrounds and is much larger than the primary landmark. By averaging over hundreds of pixels along the boundaries of this artwork, a reference location is determined for evaluating location estimators applied to the much smaller primary landmark. The design incorporates an internal measure of location accuracy, to verify that the larger secondary landmark has been located more accurately than the Cramér–Rao lower bound for the location uncertainty of the primary landmark.

In summary, the present work establishes—for the first time—the minimum uncertainty in landmark location attainable, considering an extensive physical model of image formation. With this bound, landmark location performance maps are created to show the gap between the uncertainty achieved by practical landmark location methodologies and the uncertainty bound. Moreover, novel

landmark location estimation algorithms are introduced that achieve uncertainty levels that closely approach the Cramér–Rao lower bound. Finally, experimental results are presented to validate the theoretical findings.

## 1.3 Mathematical Symbols and Nomenclature

The discussion of landmark location accuracy will involve details of geometry expressed in several coordinate frames. A notation that captures the type of representation, the point referred to and the coordinate frame of reference will provide a compact way to discuss landmark geometry unambiguously. The notation used by J.J. Craig (1986) and others is described here and used throughout this work. Notation related to signals and estimation is also described. In addition to this section, a list of symbols is provided in Appendix A.

### 1.3.1 Coordinate Systems

Point $b$ expressed in coordinate system $A$ is given by ${}^{A}P_b$. The coordinate systems used will be:

"$w$": World coordinates ${}^{w}P_b \in \Re^3 = [{}^{w}X_b \;\; {}^{w}Y_b \;\; {}^{w}Z_b]^T$, *i.e.*, user-defined inertial coordinate system

"$c$": Camera coordinates ${}^{c}P_b \in \Re^3$, *i.e.*, coordinate system centered at the principal point of the camera/lens; the z-axis ${}^{c}Z$ lies along the principal ray of the lens

"$L$": Landmark coordinates, *i.e.*, coordinate system embedded in a landmark. Two-dimensional landmarks are considered here, so ${}^{L}P_b \in \Re^2$

"$i$": Image coordinates ${}^{i}P_b \in \Re^2$, *i.e.*, a metric coordinate system centered at the intersection of the principal ray and the imager

"$p$": Pixel coordinates ${}^{p}P_b \in \Re^2$, *i.e.*, a coordinate system co-planar with the image coordinate system, centered in the upper-left corner of the imager

Generally, points expressed in image or pixel coordinates are points in the image. For example, a point $b$ in a landmark has coordinates ${}^{L}P_b$ given by the mathematical description of the landmark, ${}^{w}P_b$ given by ${}^{L}P_b$ and the transformation between landmark and world coordinates, and point ${}^{i}P_b$ is the image of point $b$ expressed in millimeters on the imager, while ${}^{p}P_b$ is the pixel coordinates of the same image point. Some additional examples are:

${}^{w}P_b$ point "$b$" in world coordinates

$$ {}^{w}P_b = \begin{bmatrix} {}^{w}X_b \\ {}^{w}Y_b \\ {}^{w}Z_b \end{bmatrix} = {}^{w}\begin{bmatrix} X \\ Y \\ Z \end{bmatrix}_b \tag{1.1} $$

${}^{c}P_b$ point "$b$" in camera coordinates

$$ {}^{c}P_b = \begin{bmatrix} {}^{c}X_b \\ {}^{c}Y_b \\ {}^{c}Z_b \end{bmatrix} = {}^{c}\begin{bmatrix} X \\ Y \\ Z \end{bmatrix}_b \tag{1.2} $$

${}^{L}P_a$ point "$a$" in landmark coordinates

$$ {}^{L}P_a = \begin{bmatrix} {}^{L}X_a \\ {}^{L}Y_a \end{bmatrix} = {}^{L}\begin{bmatrix} X \\ Y \end{bmatrix}_a \tag{1.3} $$

### 1.3.2 Origin of the Coordinate System

The origin is a special point in a coordinate frame. The origin of coordinate frame $A$ expressed in coordinate frame $D$ is denoted as ${}^{D}P_{\underset{A}{o}}$. The upper-left subscript may be omitted when a general reference to the origin of the coordinates system is made. Several examples are:

Center of a landmark in camera coordinates:

$$ {}^{c}P_{\underset{L}{o}} = \begin{bmatrix} {}^{c}X_{\underset{L}{o}} \\ {}^{c}Y_{\underset{L}{o}} \\ {}^{c}Z_{\underset{L}{o}} \end{bmatrix} = {}^{c}\begin{bmatrix} X \\ Y \\ Z \end{bmatrix}_{\underset{L}{o}} \tag{1.4} $$

Origin of the image coordinates:

$$ P_{\underset{i}{o}} \tag{1.5} $$

The image location of the center of the landmark, expressed in pixel coordinates:

$$ {}^{p}P_{\underset{L}{o}} \tag{1.6} $$

${}^{a}\mathcal{P}_b$ Symbol ${}^{a}\mathcal{P}_b$ designates a six-dimensional pose of a coordinate frame $b$ expressed in coordinate frame $a$. An example used in the development is ${}^{c}\mathcal{P}_{\underset{L}{o}}$, which is the pose of the landmark expressed in camera coordinates:

$$ {}^{c}\mathcal{P}_{\underset{L}{o}} = [{}^{c}x \;\; {}^{c}y \;\; {}^{c}z \;\; \omega \;\; \kappa \;\; \varphi]^T \;, \tag{1.7} $$

where $[{}^{c}x \;\; {}^{c}y \;\; {}^{c}z]^T$ is the 3-DOF position of the landmark in the camera frame, and where $\omega$ = pitch, $\kappa$ = roll and $\varphi$ = yaw angles of the orientation of the landmark in the camera frame. For this work, the rotation order for the rotation from target to camera coordinates is $R = R_\kappa R_\varphi R_\omega$, where each $R$ is a $3 \times 3$ rotation matrix.

### 1.3.3 Image Formation

The following subsection describes the nomenclature and mathematical symbols that will be used at each stage of the image formation model. The image formation model is described in detail in Chapter 2.

*Landmark luminosity function:*

Function that provides the definition of the landmark geometry on the landmark plane,

$$f_L({}^L x, {}^L y) \ , \tag{1.8}$$

expressed in lumens or per unit.

*Optical flux function:*

Function representing the spatial distribution of illumination of the imager considering geometric optics:

$$H({}^i x, {}^i y) = \Phi \left( G_f \left( {}^c \mathcal{P}_{\underset{L}{o}}, f_L({}^L x, {}^L y) \right) \right) \ , \tag{1.9}$$

expressed in lux or per unit.

*Illuminance function:*

Function representing the optical flux on the imager after the addition of the diffraction phenomena:

$$E({}^i x, {}^i y) = \Xi \left( H({}^i x, {}^i y) \right) \ , \tag{1.10}$$

expressed in lux or per unit.

*Discrete analog intensity function:*

Function describing the illuminance function after spatial quantization:

$$J(i,j) = Q_s \left( E({}^i x, {}^i y) \right) \tag{1.11}$$

expressed in charge or per unit.

*Digital image:*

Function describing the discrete analog intensity function after amplitude quantization:

$$I = Q_i(J(i,j)) \ , \tag{1.12}$$

expressed in units of counts on a range determined by the A/D converter, or per unit with 1 = full scale.

### 1.3.4 Estimation Basics

Estimation is the statistical discipline that involves estimating the values of model parameters based on measured data. Much of the present work employs the tools of a multivariable statistical framework with a focus on estimation theory. The following mathematical notation is used throughout.

The true value of a given parameter vector $\theta$ is marked with a star:

$$\theta^* \,. \tag{1.13}$$

The estimated value of a given parameter $\theta$ is marked with a hat:

$$\widehat{\theta} \,. \tag{1.14}$$

The misadjustment in the estimate of a give parameter $\theta$ is marked with a tilde: $\widetilde{\theta}$; that is,

$$\widehat{\theta} = \theta^* + \widetilde{\theta} \,. \tag{1.15}$$

The measurement of a data vector $Y$ is written as: $\overline{Y}$. For each measurement $\overline{Y}$, there is an underlying but generally unknown true value, $Y^*$, and measurement error or noise, $\widetilde{Y}$, with a relationship:

$$\overline{Y} = Y^* + \widetilde{Y} \,. \tag{1.16}$$

*Examples:*

- Estimated center of landmark in image coordinates:

$$\widehat{{}^{i}P_{\underset{L}{o}}} \,. \tag{1.17}$$

- Estimated location of a point $b$ in pixel coordinates:

$${}^{p}\widehat{P}_b = {}^{p}P_b^* + {}^{p}\widetilde{P}_b \,, \tag{1.18}$$

  where ${}^{p}\widetilde{P}_b$ represents estimator error.

- Measured digital image in the presence of noise:

$$\overline{I} = Q_I(\overline{J}) = Q_I(J^* + \widetilde{J}) \,, \tag{1.19}$$

  where $\widetilde{J}$ is noise in the discrete analog intensity function and $Q_I(\cdot)$ is the intensity quantization function.

- Noise in the measurement of the digital image:

$$\widetilde{I} = I^* - \overline{I} \,. \tag{1.20}$$

### 1.3.5 Estimators

The landmark location estimators are algorithms that take image data and produce a landmark location estimate, written ${}^{p}\widehat{P}_0 = T\left(\overline{I}\right)$. Four landmark location estimators are considered; these are denoted by $T_A(\,)$, $T_B(\,)$, $T_D(\,)$, and $T_E(\,)$, where:

$T_A(\,)$ is the binary centroid estimator;
$T_B(\,)$ is the grayscale centroid estimator;
$T_D(\,)$ is the ellipsoidal contour estimator, and;
$T_E(\,)$ is the Butterworth tepuy estimator.

Some nomenclature examples for estimators follow:

- Binary centroid estimator on the discrete analog intensity function $J$:

$$ {}^{p}\widehat{P}_{\underset{L}{o}} = T_A(J)\ . \tag{1.21} $$

- Butterworth tepuy estimator applied to the digital image function $I$:

$$ {}^{p}\widehat{P}_{\underset{L}{o}} = T_E(I)\ . \tag{1.22} $$

- Estimate of the center of the landmark in pixel coordinates using the ellipsoidal estimator:

$$ {}^{p}\widehat{P}_{\underset{L}{o}} = T_D(I)\ . \tag{1.23} $$

## 1.4 Content Organization

The subsequent chapters are organized as follows. Chapter 2 addresses modeling issues, with the extensive physical model of digital image formation developed in Section 2.1. Locales and the use of confidence intervals are discussed in Section 2.2. The necessary analytic tools are developed in Chapter 3, with tools for forming the confidence interval based on the Cramér–Rao lower bound derived in Section 3.1 and tools for analyzing the performance of practical estimators derived in Section 3.2. The details of two new, model-based landmark location estimators are presented in Chapter 4. Calculation of both the CRLB and practical estimator performance requires an innovation in 2-D numerical integration, which is the topic of Chapter 5. The computational tool that generates the landmark location uncertainty performance maps is presented in Chapter 6. In Chapter 7 an experimental method is presented which can directly and accurately measure the uncertainty in locating a primary landmark, based on the estimated location of a much larger and more accurate secondary landmark. This is followed in Chapter 8 by the presentation of experimentally measured landmark location uncertainty, which is used to validate the analytic tools of Chapter 3, as well as the results from numerical investigations employing the analytic tools to study the impact on location accuracy of a range of configuration variables. Finally, the conclusions of this work are presented in Chapter 9.

A downloadable MATLAB® package to assist the reader with applying theoretically-derived results to practical engineering configurations is available from http://www.springer.com/978-1-84628-912-5.

http://www.springer.com/978-1-84628-912-5

Precision Landmark Location for Machine Vision and Photogrammetry
Finding and Achieving the Maximum Possible Accuracy
Gutierrez, J.A.; Armstrong, B.S.R.
2008, XI, 162 p. With online files/update., Hardcover
ISBN: 978-1-84628-912-5